Biosensors and Bioelectronics 133 (2019) 236–242

Contents lists available at ScienceDirect

Biosensors and Bioelectronics

journal homepage: www.elsevier.com/locate/bios

Target trapping and in situ single-cell genetic marker detection with a focused optical beam

Hengji Cong[a], Fong-Chuen Loo[a,b,*], Jiajie Chen[a,*], Yuye Wang[a], Siu-Kai Kong[b], Ho-Pui Ho[a,*]

[a] Department of Biomedical Engineering, The Chinese University of Hong Kong, Hong Kong, China
[b] Biochemistry Programme, School of Life Sciences, The Chinese University of Hong Kong, Hong Kong, China

ARTICLE INFO

Keywords:
Optothermal effect
Micro-well array
Single cell trapping
DNA amplification

ABSTRACT

Optical trapping of single particles or cells with the capability of in situ bio-sensing or genetic profiling opens the possibility of rapid screening of biological specimens. However, common optical tweezers suffer from the lack of long-range forces. Consequently, their application areas are predominantly limited to target manipulation instead of biological diagnostics. To solve this problem, we herein report an all-in-one approach by combining optical forces and convective drag forces generated through localized optothermal effect for long-range target manipulation. The device consists of a 2D array of gold coated polydimethylsiloxane (PDMS) micro-wells, which are immersed by colloidal particles or cell solution. Upon excitation of a 785-nm laser, the hydrodynamic convective force and optical forces will drag the targets of interest into their designated micro-wells. Moreover, the plasmonic thermal dissipation provides a constant temperature environment for following cell analysis procedures of cell isolation, lysis and isothermal nucleic acid amplification for the detection of genetic markers. With the merits of fabrication simplicity, short sample-to-answer cycle time and the compatibility with optical microscopes, the reported technique offers an attractive and highly versatile approach for on-site single cell analysis systems.

1. Introduction

The optothermal effect, which converts photon energy into heat, is now widely used in microfluidic systems for various applications. For example, under laser illumination, a surface bubble can be generated at the interface of the liquid and the laser-absorbing surface. By controlling the bubble size and position, various actuation effects have been demonstrated, including manipulation of particles (Zheng et al., 2011; Zhao et al., 2014), cells (Hu et al., 2013) and single DNA strands (Fujii et al., 2010), switching of micro-valves and micro-pumps (Zhang et al., 2011), deformation of nanowires (Huang et al., 2010), or fabrication of plasmonic nanostructures (Karim et al., 2018). Laser-induced thermal effects also result in convective flows in the fluidic sample. Marangoni convection, which occurs at the interface between two fluids and is caused by changes in surface tension as a result of localized laser heating, has also been investigated theoretically and experimentally (Chraïbi and Delville, 2012; Near and Liquid, 2004). For solid surfaces, natural convection arises from liquid dilatation in the laser heating spot, together with thermophoresis, which is due to the presence of temperature gradient, provide many application opportunities in microfluidic systems (Flores-Flores et al., 2015; Kang et al., 2015a; Braun and Libchaber, 2002; Duhr and Braun, 2005; Lin et al., 2017). For example, we have previously reported the assembling of live cells on large-scale random nano-island substrates with the assistance of convective force and thermophoretic force (Kang et al., 2015a). Braun et al. also demonstrated the trapping of DNA (Braun and Libchaber, 2002) and the formation of two-dimensional colloidal crystals (Duhr and Braun, 2005). Linhan et al. used thermophoretic tweezers to manipulate biological cells and nanoparticles (Lin et al., 2017).

During manipulation, it is important to maintain fine control of the target-of-interest. Optical tweezers, a powerful tool to manipulate small particles and cells, have been integrated with a variety of biological systems due to its high spatial resolution, non-contact and non-invasive characteristics. However, current techniques based on optical tweezers do not provide any trapping forces when the target is no longer in the vicinity of the optical focal point. On the other hand, polydimethylsiloxane (PDMS) micro-well arrays are widely used for gravity-assisted cell confinement with diluted cell suspensions because the trapped cells are not easily dislodged after falling into a micro-well. Additionally, PDMS is a promising candidate for lab-on-a-chip (LOAC) devices because of its biocompatibility, flexibility, and ease of prototyping. Combining optical tweezers with these PDMS micro-well arrays,

* Corresponding authors.
E-mail addresses: jackyfcloo@cuhk.edu.hk (F.-C. Loo), jjchen@alumni.cuhk.net (J. Chen), aaron.ho@cuhk.edu.hk (H.-P. Ho).

https://doi.org/10.1016/j.bios.2019.02.009
Received 15 December 2018; Received in revised form 4 February 2019; Accepted 12 February 2019
Available online 28 February 2019
0956-5663/

an active manipulation in the three-dimensional level, including pull-and-push of the target, in-and-out from a micro-well can be achieved.

Not only for cell isolation, PDMS micro-well arrays are also attractive for bio-related applications including single-cell trapping and imaging (Rettig and Folch, 2005; Wood et al., 2010), stem cell culturing (Moeller et al., 2008), agarose droplet generation (Li et al., 2018) and digital PCR analysis (White et al., 2013; Schneider et al., 2013). Here we deposited a layer of gold thin film on a PDMS micro-well array. After cell confinement inside a micro-well, we further show the cellular responses under various ambient conditions, which includes cell killing in a constant high temperature generated by laser-induced optothermal effect.

Nucleic acid is well-known as the "fingerprint" to reveal the identity and property of a cell. Due to the low concentration of the nucleic acid marker from a single cell, the detection is commonly assisted by DNA amplification such as polymerase chain reaction (PCR) that targets on a particular DNA marker sequence (Hahn et al., 2000). Despite of its high sensitivity, PCR has a strict requirement for thermal cyclers, which increases the detection complexity and cost. As a result, recombinase polymerase amplification (RPA) is frequently used for rapid amplification and detection of nucleic acids in isothermal environment since no thermal cycles are needed and the reaction time can be greatly reduced. In our case, this high temperature generated form laser heating can be employed for RPA reaction of nucleic acid markers within the same setup. This approach is favorable for biomedical applications, as the cell-of-interest within the same reaction chamber can be observed and manipulated simultaneously under an optical microscope with low laser power. The turnaround time of the whole procedure is less than one hour.

2. Material and methods

A standard photolithography process was used to make a mold for the fabrication of PDMS micro-well replicas. Briefly, a silicon substrate, after ultrasonic cleaning by acetone, isopropanol, and deionized water, was placed in a plasma cleaner (Oxford Plasma Lab) to ensure that the surface was free from contaminants. Photoresist SU-8 was coated on the substrate, followed by soft baking, mask alignment, UV exposure, post-exposure baking, and photoresist development. The completed SU-8 mold comprised of 10 × 10 cuboids, each having a side length of 80 μm and a height of 60 μm. 1 mL of PDMS was poured into the SU-8 mold. After putting the PDMS-filled mold into a vacuum chamber in about 20 min to degas the bubbles and on a hot plate for 60 min to allow solidification, the cured PDMS replica was removed from the mold and placed upside down on a glass slide. A coating of nominally 30-nm thick Au was deposited on the PDMS replica using plasma sputtering process by Anatech Magnetron Sputtering Machine. As depicted in Fig. 1(a), the final device had a gold coating deposited at the bottom of each micro-well. The 2D array and a PDMS open-top microfluidic channel plate (prefabricated from another PMMA mold curved by a Computer Numeric Control (CNC) machine) were glued to the glass slide by placing them on a layer of partially-cured spin-on PDMS film on the glass slide. A schematic of the completed device is shown in Fig. 1(b). To make the micro-well-array hydrophilic, we treated the surface of the entire device with oxygen plasma (Oxford Plasma Lab).

As is shown in Fig. 1(c), the experiments were conducted under continuous monitoring with a Nikon inverted microscope (TE2000-U). A peristaltic pump was used for fluidic sample circulation and device cleaning. To introduce heating inside each well, a linearly polarized laser (λ = 785 nm, DeltaNu ExamineR 785) was chosen to illuminate the plasmonic gold film. The diameter of the laser spot was 12 μm and the output power was adjustable in five levels, i.e. P1 to P5: 1.1, 4.4, 9.2, 16.0 and 40.0 mW. A 488 nm laser was used for confocal imaging and a 532 nm-laser (Changchun New Industries Optoelectronics Tech Co., Ltd.) was for temperature detection, as will be discussed later.

To demonstrate single-cell manipulation and analysis, suspended living human leukemia cancer cells obtained from ATCC were used. The cells were prepared under standard culture conditions, i.e. RPMI 1640 medium at pH 7.4 as nutrient with incubation at 37 °C and 5% CO_2 until log phase growth for the downstream assay. The RPMI 1640 medium was removed by centrifugation and the cell was washed with distilled water prior to the experiment to remove the inhibitory factor on downstream DNA amplification. The cell was injected to the micro-well array and guided to the target micro-well with the use of laser illumination at P4 (16.0 mW) from 0 to 1 min in 20-second time intervals at the region next to the cell. The single cell fell to the bottom of the micro-well by gravity when it entered the micro-well. Afterwards, excess cells were washed away and the laser was focused at the trapped cell for 60 s, which resulted in cell lysis that could be monitored by observing cell swelling and membrane disruption. For the DNA marker detection, isothermal recombinase polymerase DNA amplification was employed. The RPA mixture used in our experiment contains recombinase, polymerase, a buffer sparked with magnesium as a co-factor to activate the enzymes and fluorescence reporter SYTO-9. The DNA marker to be detected was a multidrug-resistant gene marker related to an ATP-binding cassette transporter that exhibits the function of a membrane-bound protein to efflux the anti-cancer drug out of the cell. The operation temperature was set at 40–42 °C, which provided an optimal enzyme activity on DNA amplification speed, for a total of 30 min. The fluorescence signal was recorded and analyzed, where the net fluorescence signal on the amplified DNA was obtained by subtracting the fluorescence signal between 0 and 30 min.

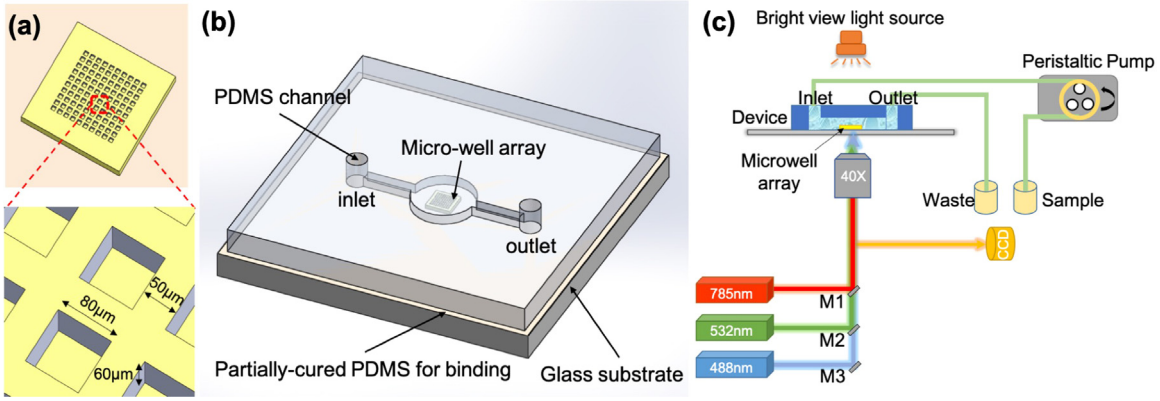

Fig. 1. (a) Schematic of micro-well array coated with a gold film. Each well has a side length of 80 μm and a height of 60 μm. (b) Schematic of a typical device with the 2D micro-well array placed inside a fluidic channel. (c) Optical measurement setup, with a 785-nm laser for heat generation, a 488-nm laser for confocal imaging and a 532-nm laser for temperature detection.

3. Results and discussion

3.1. Characterization of optothermal effect in micro-well arrays

When a focused infrared laser impinges at the gold film in the bottom of the micro-well, the temperature around the beam spot increases due to plasmonic absorption, which results in fluidic convection inside the micro-well. We show herein that convective flow generated this way can be used for manipulating micro-sized particles or cells. More importantly, the convective flow will bring the liquid from far away to the center continuously in order to reach a temperature equilibrium. In our case, each micro-well works as a heating chamber for biological reactions including isothermal recombinase polymerase amplification.

To measure the temperature inside the micro-well, we used Rhodamine B as a thermally sensitive indicator due to its dynamic quenching under different temperatures. Before monitoring the temperature of laser heating, a calibration test was conducted with a temperature-controlled stage. A device filled with Rhodamine B (10 mM) was put on the stage and the temperature was gradually increased from 20 to 60 °C, in steps of 5 °C. For each temperature, it took approximately 10 min to reach steady state. Then we captured the images of Rhodamine B under the excitation of a 532 nm green laser. The relationship between temperature T and intensity was fitted to a second order polynomial: $T(°C) = a + bx + cx^2$, where a, b, c are constants and x is the intensity ratio for a real-time temperature compared with a reference value measured at room temperature (Paviolo et al., 2013). From our experiments, it was found that a = 216.6725, b = −253.2768, and c = 58.3739. The coefficient of determination R^2 for this equation is 0.9862. We then removed the temperature-controlled stage and used a focused 785 nm laser beam as the heating source. The intensity ratios measured at different power levels were analyzed to obtain the temperature distribution, according to the temperature-intensity equation above. Intensity of Rhodamine B at the same laser power was detected repeatedly when the aqueous solution was absolutely cooled down. It turns out the difference of stable intensities after same-powered plasmonic heating is negligible, suggesting photobleaching could be excluded, which is consistent with Paviolo's work (Paviolo et al., 2013).

To gain a better understanding of the temperature environment inside the micro-well, we calculated the temperature distribution using COMSOL Multiphysics Software. To simplify the simulation, we chose a cylindrical model to represent the micro-well structure in light of its rotational symmetry. The flow was assumed to be incompressible and treated with Boussinesq approximation. As one can see from Fig. 2(a), a focused 9.2 mW (P3) Gaussian beam impinging at the center of the gold film results in a peak temperature of around 311 K, which gradually decays to 301 K. The simulated temperature decay plots along the radius for different laser levels are plotted in Fig. 2(b). As the laser power increases, the peak temperature rises from 295.5 K (P1) to 356.4 K (P5). Data shown in Fig. 2(c) confirms that simulated results are in good agreement with those obtained from experiments. Most of our experiments were conducted with laser power at P3 or below, i.e. maximum peak temperature of 312.8 K from Rhodamine B experiments or 311.4 K from simulation.

3.2. Particle manipulation in three-dimensional level

Laser-induced plasmonic heating, consisting of a metallic thin film on top of a glass substrate, has been previously reported to manipulate colloidal particles and biological cells (Lin et al., 2018; Chen et al., 2015). However, these reports are focused on target manipulation at a two-dimensional level. Rather than limiting particle motion on a planer surface, we herein showed the manipulation of a single particle in and out of a micro-well by controlling the laser beam.

Laser manipulation of target is illustrated in Fig. 3(g), where the particle of interest has gone through a sequence of steps, from (a) to (f), which have been clearly shown in the images of Fig. 3(a) to (f) respectively, can be divided into four stages: (1) Particle rises from the bottom to the top surface of the micro-well due to optical scattering force, i.e. steps (a) to (b). (2) Particle is dragged to the outside surface by optical gradient force, together with a radial convective force, i.e. steps (b) to (c). (3) Optical gradient force exerted on the particle guides the particle into the micro-well again, i.e. steps (c) to (d). (4) Particle returns to the bottom under the influence of gravity, i.e. steps (e) to (f). In support of the illustration, the experiment on three-dimensional particle trapping and manipulation was conducted, as shown in Fig. 3(a)-(f). In the actual experiment, three 10-μm polystyrene particles were distributed randomly at the bottom of a micro-well. When the laser was switched on at P3 and the beam was moved to the left one particle in Fig. 3(b), the particle would float out of the focal plane. When the particle reached the top of the micro-well, the laser spot was moved to one point on the outside surface, close to the micro-well edge. The particle, guided by the laser beam, migrated out of the micro-well. Once we moved the laser beam back into the micro-well, the particle also returned to the position of the laser spot in the x-y plane. After the laser was switched off, the single particle would drop down to the bottom due to gravity force.

To investigate the forces that contributed to the movement of the particle, we performed the same experiment using a PDMS micro-well array without any Au deposition as the negative control. As soon as the laser power was increased to P3 and the laser was focused on a particle lying at the bottom of the micro-well, the particle immediately rose up along the vertical direction. Similar to the process shown in Fig. 3, we successfully guided a particle from one micro-well into the adjacent one, thus illustrating that optical force played a major role in the particle manipulation process (Supplementary Fig. S1).

For fine-control of particle position inside a micro-well, we demonstrate that stable trapping of 1-μm polystyrene particles (1.82×10^8 particle/mL) inside a gold-coated PDMS micro-well. As shown in Fig. 4(a), the 785 nm laser was focused at the bottom surface of one micro-well (highlighted by a box in white dash line). The power was set at P2 (4.4 mW). Particles were dragged and moved by the laser spot so that a cluster was formed gradually. Because of the presence of laser-heating induced dragging forces, it was possible to move the cluster by deflecting the laser spot. As soon as we switched off the laser, the cluster of particles would disperse and return to a randomly distributed situation within a few minutes. Fig. 4(b) shows the cut-plane of flow velocity streamline at x = 0. As one can see, the convective flow has a typical toroidal shape with the fluid being pushed into and out of the hot zone. It is the radial flow that dominates the gathering of particles at the center of the laser-illuminated region. However, we also found that at higher power levels (P3, P4 or P5), the 1-μm particles were carried by the convective flow to the laser-illuminated region from a distance but did not stay trapped as the upward convective flow became too strong.

The mechanism behind the trapping phenomenon has been investigated in our preliminary work (Kang et al., 2015b). The high temperature first leads to a natural convection flow driven by buoyancy. In this case, particles close to the film surface can be dragged towards the center of the hot zone by convective force. On the other hand, because of the inhomogeneity at the particle-solvent interface induced by a temperature gradient, another force named as thermophoretic force, drives the particle towards the hot or cold side, depending on various parameters such as particle size, temperature and electrolyte composition (Cong et al., 2018). With our experiment performed at laser power P2, the thermophoretic force pointing towards the hot region, together with the optical near-field force, resulted in a net trapping force and immobilized the particles at the beam spot. If we increased the power level beyond P2, the particle cluster began to disperse as convective forces exceeded the trapping force due to thermophoresis and optical localization. As long as the laser beam at power

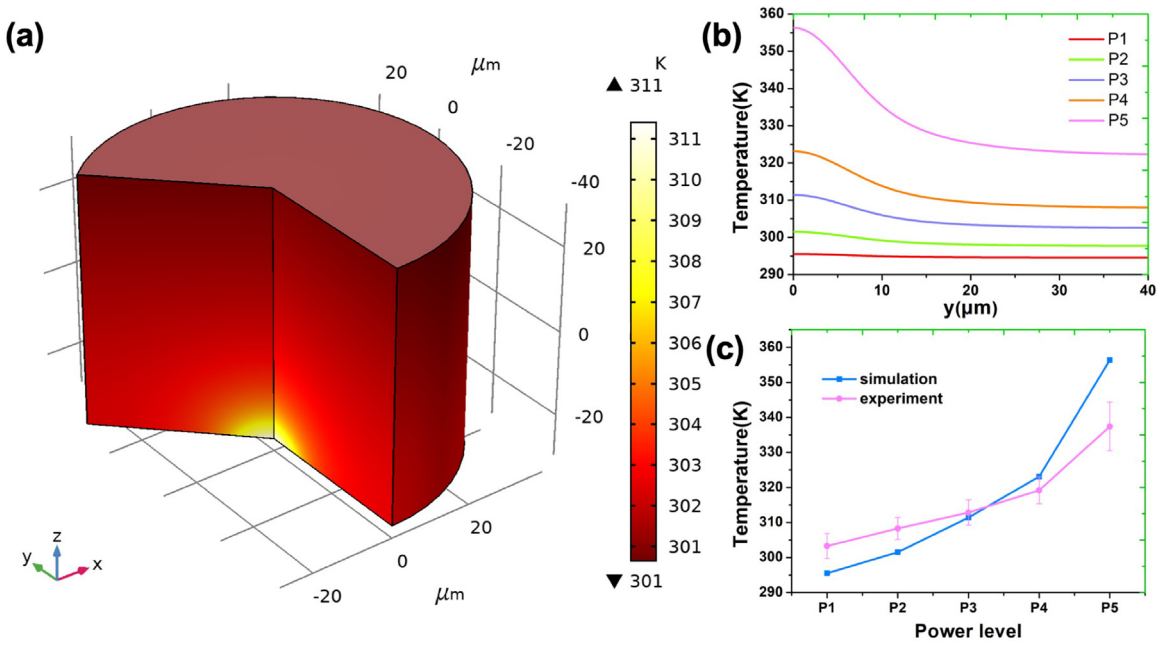

Fig. 2. Temperature distribution inside a micro-well. (a) Temperature distribution when the laser power was set at P3. (b) Temperature along y-axis at x = 0 and z = 0, from P1 to P5. (c) Comparison between simulated and experimental results.

level P2 was present, the particles remained in trapped state inside the micro-well. For particles in other micro-wells, apart from localized vibration due to Brownian motions, they did not exhibit any changes even for a long period. Therefore, each micro-well in the 2D array may function as an individual reaction chamber.

3.3. Manipulation and analysis of single cells

Single cell analysis is meaningful for in-depth study of cell-to-cell variation and intracellular process. Many techniques have been reported for the isolation of single cells from a dense cell suspension without integrity damage, including fluorescence-activated cell sorting (FACS) (Hahn et al., 2000), limiting dilution (Quintana et al., 2008), micromanipulation (Ishøy et al., 2006), manual picking (Citri et al., 2012)and microfluidics (Oakey et al., 2002). Taking the advantage of optical tweezer for cell manipulation and PDMS micro-wells for cell confinement, our setup is also capable of precisely isolating cells, which is an essential step in single cell detection. To demonstrate the practical application potential of the reported approach, we have used the setup to perform cell analysis on suspended living human leukemia cancer cells. Indeed, the mean diameter of the cell is close to the 10-μm particles so that we could observe a similar trapping pattern compared to that with particles. As shown in Fig. 5(a), to induce movement of the individual cell, an optical beam at P3 is focused adjacent to the cell to create a convective flow that drags the cell to the center of the optical beam. After the cell was tightly confined by the focused laser, it was guided into a targeted micro-well from the top region by sequentially controlling the laser power and location, similar to the characterization on step (c)-(f) using a particle shown in Fig. 3.

The optothermal effect which yields a localized high temperature on the gold surface could also cause swelling of the cell when a living cell is exposed directly to the focused optical beam. Fig. 5(b) shows the process of membrane swelling in a single cancer cell during 60 s of laser heating at P4. After the single cell fell to the bottom surface for a while, the adhesion between cell and gold surface would keep it immobilized even at a high laser power like P4. But the high temperature denatured the membrane-bound proteins and reduced the fluidity of the cell lipid membrane. As a result, the intracellular contents including the nucleic

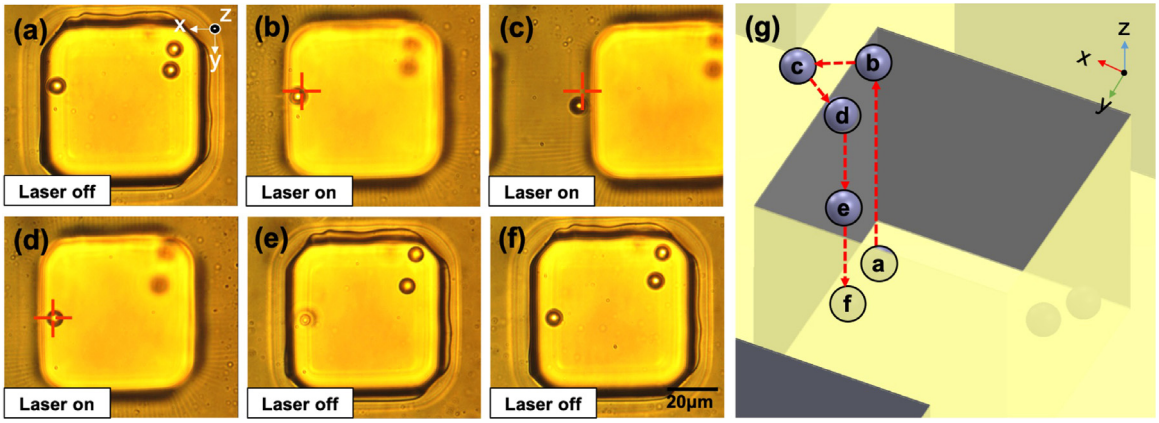

Fig. 3. Guiding of a single-particle in-and-out of a gold-coated micro-well by controlling the power and illumination location of the laser spot. (a) Three particles distributed randomly at the bottom. (b) Guiding a particle out of micro-well by moving the laser spot. (c) The particle is placed at the top edge of micro-well. (d) Particle re-entered micro-well under the manipulation by laser spot. (e-f) Particle fell to the bottom of micro-well under the influence of gravity. (g) Schematic summarizing the steps shown in (a) to (f).

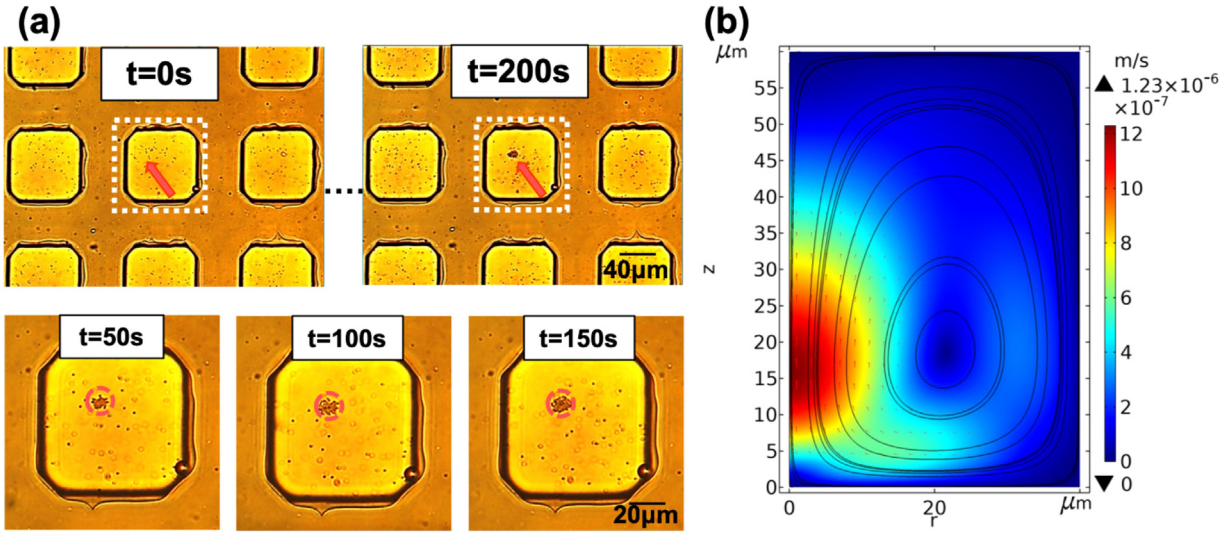

Fig. 4. (a) Particle trapping inside a gold-coated micro-well under laser heating. The power was set at P2. (b) Streamline of velocity field inside the micro-well.

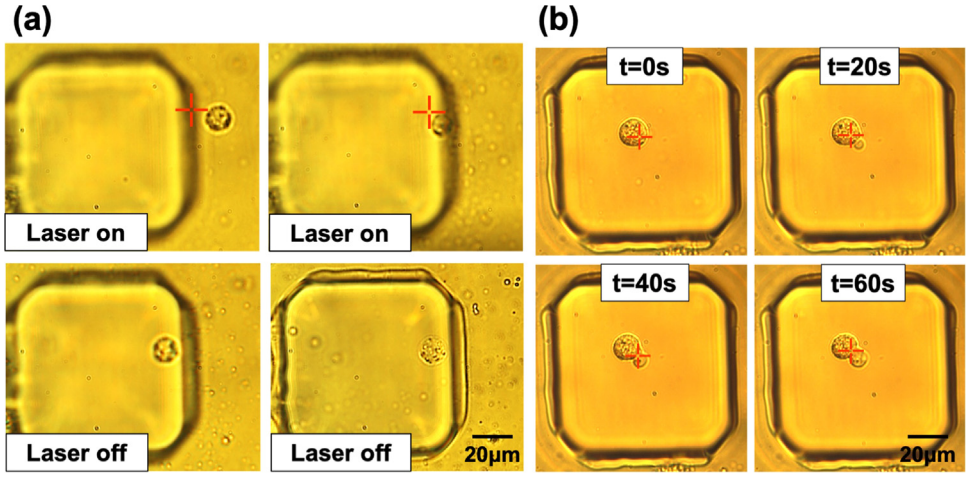

Fig. 5. Manipulation of a single cancer cell. (a) Optical guiding of a free-flowing living single cancer cell into a micro-well. (b) Time-lapse images showing cell lysis during the first 60 s of laser illumination directed at the cell membrane.

acid were released. The "bubble" generated at the right bottom of the cell in Fig. 5(b) indicated the cell disruption under laser-induced thermal effect. In this case, this is the temperature-induced membrane disruption and cell damage instead of apoptosis, as the same phenomenon was appeared in seconds rather than minutes. Indeed, DNA fragmentation degrades the target DNA marker during apoptosis, and it will cause false negative signal in our detection method. Since we did not observe such interference, it suggested the cell necrosis was the major mechanism for this laser-induced cell death. The increasing size of the "bubble" with time suggested that the intracellular content was continuously leaking from the cell, where the released DNA enabled the downstream cell biomarker detection. Worth to notice, the laser focus region was at the edge of the cell, i.e. the cell membrane region, it minimized the effect of laser-induced heating to the intracellular content. Indeed, heating could denature the enzyme which degraded the DNA. This cell lysis procedure was believed not to generate undesirable products which affected the downstream DNA amplification. In all, this laser-induced heating effect in our study provides an alternative method for rapid cell disruption, which is supported by other reported laser-induced cell lysis methods (Brown and Audet, 2008; Quinto-Su et al., 2008).

Optothermal effect also works as an ideal method for amplification of DNA in bio-systems, like real-time PCR in nanodroplets (Kim et al., 2009) or ultrafast PCR in poly(dimethylsiloxane) (PMMA) wells (Son et al., 2015). In this study, Recombinase Polymerase amplification (RPA), an isothermal alternative to PCR that is optimized at 25–45 °C, was used here to detect multidrug-resistant gene marker, which has led to a high failure in current leukemia cancer treatment with first-line arsenic-based anti-cancer drug (Loo et al., 2013; Xu et al., 2013). Also, since the released DNA could be double-strand or single-strand in nature in the experiment, the RPA reaction containing the enzyme that displaced the compliment strand from the target strand that was bound to the primer could enable the reaction to occur at a relatively low temperature (37 °C) compared to normal DNA amplification (PCR) which required a high temperature (95 °C) for DNA denaturation step, in order to turn double-strand DNA into single-strand for enzyme binding.

We first demonstrated the capacity of optically-guide DNA amplification in a particular micro-well. After DNA, premixed with RPA reaction mixture, was loaded to fill the micro-well, the excess mixture was removed with a layer of mineral oil to isolate each micro-well, as shown in Fig. 6(a), so that the amplified DNA would not leak to other micro-wells. Localized heating was applied on a particular micro-well and an increase in green fluorescence (0.81 ± 0.09 A.U.) suggested there was target DNA amplification inside the micro-well (Fig. 6(b)). Relative fluorescence intensity of different wells is calculated (Fig.

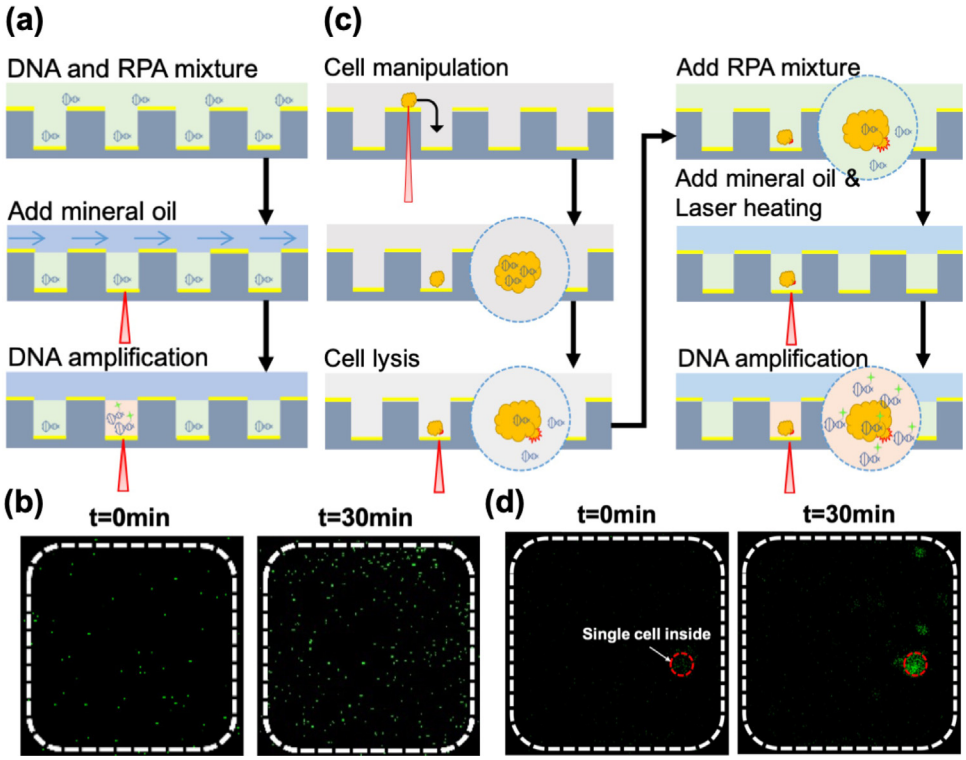

Fig. 6. Selective DNA amplification in a single micro-well. (a) Schematic diagram showing the procedures of DNA amplification in a particular micro-well. (b) Fluorescence image of the 0 and 30-min RPA reaction. (c) Schematic diagram showing the procedures for DNA amplification of a targeted cancer cell. (d) Fluorescence image showing amplified DNA of a single cell inside the micro-well at 0 and 30-min RPA reaction.

S2(a) in Supplementary materials) and it is worth noting that the intensity of green fluorescence also slightly increased in the adjacent wells (0.26 ± 0.09 A.U.) during plasmonic heating. Since the distance between wells is closer in this design, the laser spot was found to have scattered to the adjacent wells. Although the power is not high enough for plasmonic trapping, it increases the temperature in the nearby well, causing DNA amplification. The experiment was repeated with loading the micro-well array with dye-stained particles. Fluorescence intensities inside and outside a micro-well with and without the use of mineral oil were measured (Fig. S2(b) in Supplemental materials). The low fluorescence intensity (0.10 ± 0.04 A.U.), which is close to background fluorescence, observed in the peripheral region surrounding the micro-well suggests the use of mineral oil is an effective way to prevent contamination of the material such as particles and DNA flowing from the target micro-well to peripheral environment. To provide a multiplex particle and cell manipulation, i.e. trapping and cell lysis, in multiple wells at the same time, digital micromirror device (DMD) can be used to generate a spatially modulated laser beam in an accurate and precise manner.

After a successful demonstration of optically-guided DNA amplification in a single micro-well, we further conducted a complete sample-to-answer experiment for single cell manipulation and genetic marker detection. As shown in Fig. 6(c), after the targeted cell was guided into a micro-well of interest and disrupted using high-power laser heating for single cell lysis, RPA mixture was loaded and the optically-guided DNA amplification was performed using laser power at P3 to result in a temperature of around 40 °C, for RPA of the target DNA marker inside the micro-well. In Fig. 6(d), the relative fluorescence intensity was increased from 0.2 to 1.0 after 30-min laser-induced heating, suggesting there was an increase in number of amplified DNA belonged to the target cancer cell after the RPA reaction. The amplification is indeed specific to the multidrug-resistant gene of the cancer cell, and the cell-of-interest showing the fluorescence suggested the presence of its gene. RPA is the reason for the signal increase since the fluorescence reporter only produces fluorescence upon binding to the amplicon DNA. Although it cannot replace the sequencing technique to valid the detail of the multidrug-resistant gene, it provides a rapid mean to screen if the cancer cell contains multidrug-resistant marker. The optothermal effect providing a steady high temperature at 40–42 °C enables an isothermal amplification, not only provides an optimal temperature for the amplification reaction, but also increases the specificity of primer binding for target gene detection.

This method has achieved single cell detection in a reaction volume of 0.38 nL inside a micro-well within a 30-min reaction. The detection limit of this single cell DNA analysis could not be analyzed currently since we did not study the copy number of the target DNA in one cell. The copy number of the target DNA in genomic DNA should be single, but we could not exclude the duplication of chromosome in cell-division cycle, and the target DNA could also present in other locations of the cell. Other studies employing RPA in miniaturized microfluidic analysis systems for sensitive DNA detection have achieved detection limits of as low as 10 copies, or 1 fg of the target DNA in various reaction volumes, from 9 nL to 20 μL, and the reaction could be completed in less than 20 min (Lutz et al., 2010; Shen et al., 2011; Law et al., 2018). Nevertheless, this experiment successfully demonstrated the presence of amplified DNA at a microscopic level within the same micro-well, immediately following lysing the cell using the same laser source.

4. Conclusion

We have developed a strategy to (i) manipulate the movement of micro-sized objects in and out of individual micro-wells based on localized plasmonic heating and optical trapping, (ii) perform analysis of cells through localized cell lysis and at-the-spot microscopic nucleic acid amplification of target DNA markers within the same platform. In our system, the laser beam serves as an optical tweezer as well as a heat source, which significantly simplifies the procedures for single cell manipulation-and-analysis. Through adjusting the laser power and illumination location, one can optimize the balance between the long-range optothermal effect generated at the gold surface and short-range optical forces for a 3D control of micro-sized objects to the target location. After capturing a single cell in a micro-well, one can perform cell lysis by increasing the laser power. Through isothermal DNA

amplification within a stable temperature profile generated by the steady-state laser beam, we have successfully demonstrated cell identification by detecting their DNA fingerprint. Here we only carried out single cell analysis in one micro-well. In order to increase the efficiency and productivity of this design, future work would be focused on deflecting the laser beam into multiple wells for a series of laser heating and DNA detection simultaneously. Overall, the reported technique makes the best use of an optical platform and a gold-coated micro-well array for setting up a workflow that covers all single cell analysis procedures including single cell confinement, cell disruption and DNA amplification, which may bring new insights on the future design of bio-chips and integration of sample-to-answer instruments.

CRediT authorship contribution statement

Hengji Cong: Conceptualization, Methodology, Investigation, Data curation, Visualization, Writing - original draft. **Fong-Chuen Loo:** Conceptualization, Methodology, Investigation, Writing - original draft, Project administration. **Jiajie Chen:** Conceptualization, Software, Methodology, Writing - original draft, Project administration. **Yuye Wang:** Formal analysis, Validation, Writing - review & editing. **Siu-Kai Kong:** Resources, Funding acquisition. **Ho-Pui Ho:** Resources, Writing - review & editing, Supervision, Funding acquisition, Project administration.

Acknowledgement

The authors wish to acknowledge funding support from the Research Grants Council, University Grants Committee HKSAR, through projects under General Research Fund (14210517) and Area of Excellence (AoE/P-02/12). We also gratefully acknowledge a postgraduate research studentship (Hengji Cong) awarded by The Chinese University of Hong Kong.

Declaration of interests

None.

Appendix A. Supporting information

Supplementary data associated with this article can be found in the online version at doi:10.1016/j.bios.2019.02.009.

References

Braun, D., Libchaber, A., 2002. Phys. Rev. Lett. 89, 188103.
Brown, R.B., Audet, J., 2008. J. R. Soc. Interface 5, S131–S138.
Chen, J., Kang, Z., Wang, G., Loo, J.F.C., Kong, S.K., Ho, H.-P., 2015. Lab Chip 15, 2504–2512.
Chraïbi, H., Delville, J.P., 2012. Phys. Fluids 24, 032102.
Citri, A., Pang, Z.P., Südhof, T.C., Wernig, M., Malenka, R.C., 2012. Nat. Protoc. 7, 118–127.
Cong, H., Chen, J., Ho, H.P., 2018. Sens. Actuators B Chem. 264, 224–233.
Duhr, S., Braun, D., 2005. Appl. Phys. Lett. 86, 131921.
Flores-Flores, E., Torres-Hurtado, S.A., Páez, R., Ruiz, U., Beltrán-Pérez, G., Neale, S.L., Ramirez-San-Juan, J.C., Ramos-García, R., 2015. Biomed. Opt. Express 6, 4079–4087.
Fujii, S., Kobayashi, K., Kanaizuka, K., Okamoto, T., Toyabe, S., Muneyuki, E., Haga, M., 2010. Chem. Lett. 39, 92–93.
Hahn, S., Zhong, X.Y., Troeger, C., Burgemeister, R., Gloning, K., Holzgreve, W., 2000. Cell. Mol. Life Sci. 57, 96–105.
Hu, W., Fan, Q., Ohta, A.T., 2013. Lab Chip 13, 2285–2291.
Huang, X., Quinto-Su, P.A., Gonzalez-Avila, S.R., Wu, T., Ohl, C.D., 2010. Nano Lett. 10, 3846–3851.
Ishøy, T., Kvist, T., Westermann, P., Ahring, B.K., 2006. Appl. Microbiol. Biotechnol. 69, 510–514.
Kang, Z., Chen, J., Wu, S.-Y., Chen, K., Kong, S.-K., Yong, K.-T., Ho, H.-P., 2015a. Sci. Rep. 5, 9978.
Kang, Z., Chen, J., Wu, S.Y., Ho, H.P., 2015b. RSC Adv. 5, 105409–105415.
Karim, F., Vasquez, E.S., Zhao, C., 2018. Opt. Lett. 43, 334.
Kim, H., Dixit, S., Green, C.J., Faris, G.W., 2009. Opt. Express 17, 218.
Law, I.L.G., Loo, J.F.C., Kwok, H.C., Yeung, H.Y., Leung, C.C.H., Hui, M., Wu, S.Y., Chan, H.S., Kwan, Y.W., Ho, H.P., Kong, S.K., 2018. Anal. Biochem. 544, 98–107.
Li, X., Zhang, D., Zhang, H., Guan, Z., Song, Y., Liu, R., Zhu, Z., Yang, C., 2018. Anal. Chem. 90, 2570–2577.
Lin, L., Hill, E.H., Peng, X., Zheng, Y., 2018. Acc. Chem. Res. S1, 1465–1474.
Lin, L., Peng, X., Wei, X., Mao, Z., Xie, C., Zheng, Y., 2017. ACS Nano 11, 3147–3154.
Loo, J.F.C., Lau, P.M., Ho, H.P., Kong, S.K., 2013. Talanta 115, 159–165.
Lutz, S., Weber, P., Focke, M., Faltin, B., Hoffmann, J., Müller, C., Mark, D., Roth, G., Munday, P., Armes, N., Piepenburg, O., Zengerle, R., von Stetten, F., 2010. Lab Chip 10 (7), 887–893.
Moeller, H.C., Mian, M.K., Shrivastava, S., Chung, B.G., Khademhosseini, A., 2008. Biomaterials 29, 752–763.
Near, I., Liquid, T.H.E., 2004. J. Appl. Mech. 45, 699–704.
Oakey, J., Allely, J., Marr, D.W.M., 2002. Biotechnol. Prog. 18, 1439–1442.
Paviolo, C., Clayton, A.H.A., Mcarthur, S.L., Stoddart, P.R., 2013. J. Microsc. 250, 179–188.
Quintana, E., Shackleton, M., Sabel, M.S., Fullen, D.R., Johnson, T.M., Morrison, S.J., 2008. Nature 456, 593–598.
Quinto-Su, P.A., Lai, H.H., Yoon, H.H., Sims, C.E., Allbritton, N.L., Venugopalan, V., 2008. Lab Chip 8, 408–414.
Rettig, J.R., Folch, A., 2005. Anal. Chem. 77, 5628–5634.
Schneider, T., Yen, G.S., Thompson, A.M., Burnham, D.R., Chiu, D.T., 2013. Anal. Chem. 85, 10417–10423.
Shen, F., Davydova, E.K., Du, W., Kreutz, J.E., Piepenburg, O., Ismagilov, R.F., 2011. Anal. Chem. 83 (9), 3533–3540.
Son, J.H., Cho, B., Hong, S., Lee, S.H., Hoxha, O., Haack, A.J., Lee, L.P., 2015. Light Sci. Appl. 4.
White, A.K., Heyries, K.A., Doolin, C., Vaninsberghe, M., Hansen, C.L., 2013. Anal. Chem. 85, 7182–7190.
Wood, D.K., Weingeist, D.M., Bhatia, S.N., Engelward, B.P., 2010. Proc. Natl. Acad. Sci. USA 107, 10008–10013.
Xu, S., Zhang, Y.F., Carew, M.W., Hao, W.H., Loo, J.F.C., Naranmandura, H., Chris Le, X., 2013. Arch. Toxicol. 87, 1013–1023.
Zhang, K., Jian, A., Zhang, X., Wang, Y., Li, Z., Tam, H., 2011. Lab Chip 11, 1389.
Zhao, C., Xie, Y., Mao, Z., Zhao, Y., Rufo, J., Yang, S., Guo, F., Mai, J.D., Huang, T.J., 2014. Lab Chip 14, 384–391.
Zheng, Y., Liu, H., Wang, Y., Zhu, C., Wang, S., Cao, J., Zhu, S., 2011. Lab Chip 11, 3816–3820.